NOTE

Real-time study of the adsorption and grafting process of biomolecules by means of Bloch surface wave biosensors

A. Sinibaldi,[1‡] V. Montaño-Machado,[2‡] N. Danz,[3] P. Munzert,[3] F. Chiavaioli,[4] F. Michelotti,*[1] and D. Mantovani*[2]

[1]Department of Basic and Applied Science for Engineering, SAPIENZA University of Rome, Rome, Italy.
[2]Laboratory for Biomaterials and Bioengineering (CRC-I), Dept. of Min-Met-Materials Eng. & CHU de Quebec Research Center, Laval University, Quebec City, Canada.
[3]Fraunhofer Institute for Applied Optics and Precision Engineering IOF, Jena, Germany.
[4]Institute of Applied Physics "Nello Carrara" (IFAC), National Research Council of Italy (CNR), 50019 Sesto Fiorentino, Firenze, Italy.
*Corresponding authors: francesco.michelotti@uniroma1.it and diego.mantovani@gmn.ulaval.ca
‡These authors contributed equally to this work.

ABSTRACT: A combined label-free and fluorescence surface optical technique was used to quantify the mass deposited in binary biomolecular coatings. These coatings were constituted by fibronectin (FN), to stimulate endothelialization, and phosphorylcholine (PRC), for its hemocompatibility, which are two properties of relevance for cardiovascular applications. One dimensional photonic crystals sustaining a Bloch surface wave were used to characterize different FN/PRC coatings deposited by a combination of adsorption and grafting processes. In particular, the label-free results permitted to quantitatively assess the mass deposited in FN adsorbed (185 ng/cm^2) and grafted (160 ng/cm^2). PRC binding to grafted FN coatings was also quantified, showing a coverage as low as 10 ng/cm^2 and 12 ng/cm^2 for adsorbed and grafted PRC, respectively. Moreover, desorption of FN deposited by adsorption was detected and quantified upon the addition of PRC. The data obtained by the surface optical technique were complemented by water contact angle and XPS analyses. The results were in accordance with those obtained previously by qualitative and semi-quantitative techniques (XPS, ToF-SIMS) on several substrates (PTFE, stainless steel), confirming that grafted FN coatings show higher stability than those obtained by FN adsorption.

Characterizing the interaction of biomolecules with surfaces in real time is of high relevance to understand the biological performance of biomaterials [1,2]. Indeed, the study of the interaction of proteins with other biomolecules at surfaces can be relevant for both the conception of multi-molecule coatings and the *in vitro* assessment of the biological performance of medical devices [3–5]. Additionally, understanding these interactions is critical for the rational design of biologically active composites with sensing, biological, and electronic functions. Moreover, in order to improve the biological performance of biomaterials, several research teams have been interested in studying coatings of two biomolecules with complementary properties [4–6]. In this context, a great challenge occurs when quantifying coatings of two molecules with high difference in molecular weight. In previous works, coatings of fibronectin (FN, 450 000 g/mol) and phosphorylcholine (PRC, 184 g/mol) were reported for cardiovascular applications [7]. FN is a glycoprotein of the extracellular matrix used to stimulate the endothelialization process [4,8,9]; while PRC is the headgroup of phospholipids found in the membrane of erythrocytes, known to provide hemocompatibility properties [10–12]. In those works, PRC was detected on the surfaces in a qualitative and semi-quantitative way, mainly by Time of Flight Secondary Ion Mass Spectrometry (ToF-SIMS) and X-ray Photoelectron Spectroscopy (XPS) analyses. Moreover, speculations could be made about the addition of PRC. In the case of fibronectin coatings, the conformation of the protein and the availability of its cell binding domain (arginine–glycine–aspartic acid, RGD sequence) is crucial to promote endothelialization [13,14]. On the other hand, the presence of PRC at the outmost molecular layer is desired in order to mimic the membrane of erythrocytes and hence, to provide hemocompatibility properties [15,16]. Hence, the relevance of studying the interaction of several biomolecules on coatings for biomaterials lies on the understanding – and prediction – of the preservation of their biological properties, which should have an impact on the further biological performance of medical devices.

In the present work, a combined label-free and fluorescence surface optical technique [17] was applied to quantify - in real time - the amount of FN and PRC during the growth of binary biomolecular coatings. The technique allowed accessing quantitative data on the interaction of FN and PRC, which were deposited at a surface by means of different coating approaches. To accomplish this objective, one dimensional photonic crystal (1DPC) biochips were used. Indeed, their sensitive surface was used to grow the binary coatings. Purposely designed biochips sustain a Bloch surface wave (BSW) [18] at the interface between the 1DPC and an aqueous external medium [19]. The strongly confined electromagnetic field associated to the BSW can be used as a probe to detect biomolecular binding events in very thin layer close to the surface (about 100 nm). Recently several groups reported on the application of BSW, with several different optical sensing schemes, to the field of cancer biomarkers detection [17,20] and to the study of the conformational changes of proteins [21], which is relevant for the further understanding of the biological performance of biomaterials. Compared to the surface enhanced infrared absorption (SEIRA)[22] and surface plasmon resonance (SPR)[23] spectroscopy techniques, which exploit the excitation of surface plasmon polaritons (SPP), the main advantages of

BSW are in that their dispersion can be almost arbitrarily tuned in wavelength, momentum and polarization by changing the 1DPC materials and geometry. Typically, the resonances they show when used for label-free biosensing are much sharper due to the reduced absorption losses, resulting in an increase of sensor performances[24]. Moreover, in fluorescence applications, the emission of labels at the sensor's surface does not suffer from quenching in proximity of any metal layer.

In our sensing scheme, the surface technique can either sense the perturbation of the surface refractive index due to the growth of a biolayer at the surface (label-free, LF mode) [25,26] or collect the resonant fluorescence emission from specific labels (fluorescence, FLUO mode) [20,27]. On one hand, it had been reported that the LF mode can detect binding of biomolecules with a limit of detection LoD_{LF} = 160 pg/mm^2, in the case of cancer biomarker proteins (ErbB2) with a mass of 110-185 kDa [17]. Such LoD_{LF} is ideal for detecting large biomolecules such as FN but is not enough low to detect light molecules, such as PRC. Conversely, the FLUO mode, besides offering the possibility to confirm the protein levels measured in a LF experiment, allows accessing a much lower limit of detection LoD_{FL} = 3 pg/mm^2, which is suitable for the detection of PRC. Such a low LoD_{FL} was experimentally estimated for the same ErbB2 proteins [17] and, given that the fluorescence signal depends on the number density rather than on the mass density, is even expected to decrease for lighter biomolecules. For fluorescence operation, the binary FN/PRC coatings were allowed to react with a double-step molecular recognition system adding fluorescent labels specifically to PRC. From the surface wave enhanced fluorescence signals, it was possible to quantify the presence of PRC for different coating approaches of adsorbed and/or grafted FN and PRC molecules. This is a promising approach to detect small molecules – as PRC - in nanometric coatings, which is not trivial with conventional surface characterization techniques.

EXPERIMENTAL SECTION

1DPC sensor

1DPCs are one-dimensional layered structures with periodic distribution of low and high refractive index materials along the stacking direction [28]. These structures permit to "mold the flow of light" [29], to confine and to enhance the electric field in a high index region near the surface of the 1DPC. The 1DPCs used in the experiments were deposited either on glass slides or plastic chips by plasma ion assisted deposition under high vacuum conditions using (Leybold Optics, APS904). The deposited dielectric materials were silica (SiO_2) for the low refractive index layers, while tantala (Ta_2O_5) and titania (TiO_2) were used for the high refractive index layers. The refractive indices at λ_1 = 670 nm were determined either by reflection/transmission spectroscopy on single layers or by ellipsometry: $n(SiO_2) = 1.474 + j5\times10^{-6}$ and $n(Ta_2O_5) = 2.160 + j5\times10^{-5}$, $n(TiO_2) = 2.28 + j1.8\times10^{-3}$. Fig. 1a shows a sketch of the 1DPC used in the experiments. The dielectric multilayer was constituted by a first silica layer, a periodic part with two tantala/silica bilayers and a topping thin titania/silica bilayer. The thicknesses were $d(SiO_2)$ = 275 nm, $d(Ta_2O_5)$ = 120 nm for the periodic part and $d(TiO_2)$ = 20 nm, $d(SiO_2)$ = 20 nm for the topping layers.

Read-out system for 1DPC biochips

As it is sketched in Fig. 1b, the excitation of a BSW is obtained by illuminating the 1DPC at either λ_1 or λ_2 through a prism coupler in total internal reflection (TIR) conditions (Kretschmann-Raether) [25,30].

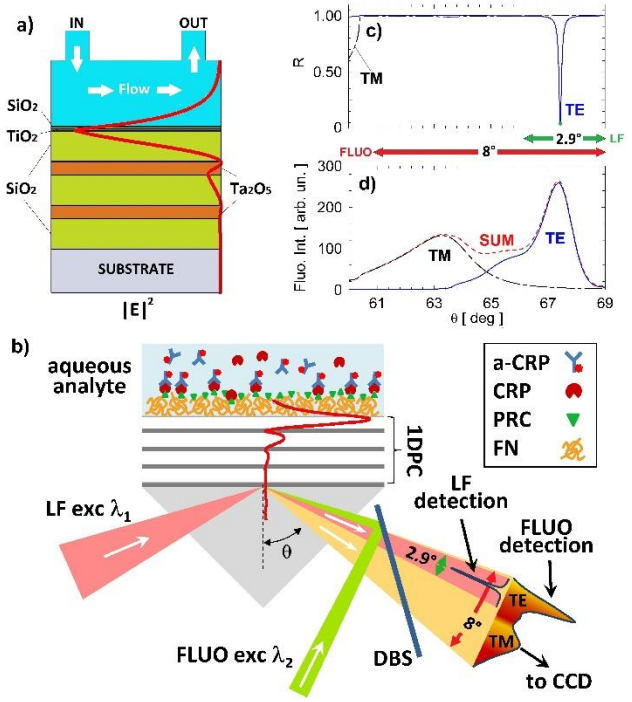

Figure 1: a) 1DPC geometry. The sensitive surface, where the intensity of the TE polarized BSW is enhanced, is in contact with the microfluidic channel that is used to inject the analytes. b) Simplified read-out configuration. Optics, filters and polarizers are not shown. c) Calculated angular reflectance at λ_1. The double green arrow marks the LF angular operating window. d) Radiant intensity calculated for isotropically oriented Dyomics 647 molecules placed at the surface of the 1DPC. The double red arrow marks the FLUO angular operating window.

Fig. 1c shows the calculated TIR angular reflectance spectrum for TE and TM polarized incident light at λ_1, when the external medium is water (n_{H2O} = 1.330). The dip in the reflectivity indicates that a BSW is excited at about θ = 67 ° when working in TE polarization. In previous works, we reported on the dependency of the dip on the 1DPC geometry[24,31,32]. In general, increasing the number of periods N leads to a narrowing of the dip and to an increase of its depth up to a maximum, followed by a decrease for large N. By tracking the shift of the angular position of the TE dip, it is possible to trace refractive index perturbations as well as molecular interactions at 1DPC surface (LF mode) [33]. The LF sensing characteristics of the 1DPC, i.e. its resonance angle, sensitivity (31.8 deg/RIU) and figure of merit, were already reported elsewhere [20].

The unique properties of the 1DPC can be exploited in the

FLUO mode as well. Illuminating the chips with a proper excitation wavelength λ_2 = 635 nm in resonant conditions yields surface wave enhanced fluorescence excitation, which transfers the maximum energy to the labelled molecules at the surface of the chip. Under such conditions, the excitation field intensity at the surface is enhanced by a factor 64 and 7, with respect to a bare substrate/liquid interface (TIR edge) and a SPR thin gold layer sensor at resonance (operating at the optimum wavelength of 810 nm), respectively. The penetration depth of the BSW evanescent field in the liquid is 103 nm. Moreover, the Stokes shifted spontaneous emission is coupled to the modes of the 1DPC, thus yielding emission in a very narrow angular range only. For the dye used as a label in the present work, Dyomics 647, the fluorescence emission calculated over an 8° angular range appears as in Fig.1d, where the overall angular spectrum shows contributions due to either the TM or TE polarized BSW sustained by the 1DPC [34]. The dye spectral emission is angularly redistributed due to the dispersion of the BSW and the enhanced fluorescence is revealed by means of the same detector used in the LF mode. In general, the TE and TM BSW could be exploited for conformational studies of proteins. In fact, depending on its orientation, an emitter will couple with a different strength to either the TE or TM mode, giving rise to a change of the relative intensities.In the practical implementation, the read-out system makes use of cylindrical optics for illumination and detection, which is not shown in Fig.1b for the sake of simplicity but were detailed elsewhere [35]. In the LF mode, the collimated and TE polarized beam of a laser diode at λ_1 is focused by a first cylindrical lens into the biochip (FWHM above 4°), thus illuminating a line at the sensor surface. The reflected light is angularly imaged onto a CCD sensor (APOGEE Ascent with Sony ICX814, 2712 rows x 3388 columns) by a second cylindrical lens, which acts as a Fourier lens. Therefore, each pixel along a row of the CCD image represents an angular component of the reflected light, with the intensity distribution shown in Fig. 1c. An angular range of 2.9° (green arrows in Figs. 1b-c) is imaged over the long dimension of the CCD. Using a telecentric cylindrical optics to image the microchannel onto the columns of the CCD enables for sensing 100 μm wide areas independently along the illuminated line, thus favoring parallel or spatially resolved analyses.

In the FLUO mode, the second collimated and TE polarized beam of a laser diode at λ_2 is focused (FWHM = 0.64°) by a cylindrical lens into the sensor in order to shine the same line as the one illuminated in the LF mode (Fig. 1b). A 45° dichroic beam splitter (DBS, long pass λ > 650 nm) is used to reflect the excitation beam and transmit the fluorescence emission, which is dispersed over an 8° angular range (red arrows in Fig. 1b-d). In such an epifluorescence configuration, excitation (band pass, 625-645 nm) and emission filters (bandpass, 650-720 nm) are used to improve the signal/noise ratio (not shown in Fig. 1b). To increase the angular range imaged by the same CCD, from the 2.9° used in the LF mode to the 8° needed in the FLUO mode, a further system of cylindrical lenses is present along the detection arm. Lateral imaging of the fluorescent spots along the illuminated line onto the CCD is provided by the same optical system as in the LF mode [20].

Binary coatings

FN/PRC binary coatings were deposited on the 1DPC surface of the biochip (Fig. 1b), while monitoring in real time the LF and FLUO signals. First, samples in which a FN layer is either adsorbed (A) or grafted (G) at the surface were prepared. Then, PRC was either adsorbed or grafted to the FN coated chips, giving rise to four possible combinations (AA, AG, GA, GG), where for example GA means FN grafted (FN_g) and PRC adsorbed (PRC_a). In all cases, sensors were previously cleaned in a piranha solution (H_2SO_4:H_2O_2, 3:1) for 10 min and stabilized the chip temperature at 37 °C during the growth of the coatings.

FN was purified from human cryoprecipitate blood plasma according to a well-established protocol [36]. The purification process resulted in a protein solution with a purity of 98 wt %. The purified FN was filtered through a 0.2 μm filter and brought to solution in the running buffer HEPES (Sigma) at 10 mM and pH 7.4, at the concentration of 50 μg/mL. Then it was stored until use at about 4-8 °C.

PRC was purchased (Sigma) and dissolved as it was immediately before use in the same running buffer at 33 mg/mL (0.1 M).

FN adsorption process (FNa): The 1DPC biochips were topped with a microfluidic cell [20] and mounted on the optical read-out system. 500 μL of running buffer were injected by means of a motorized syringe. Then, 180 μL of the FN solution were injected with a flow rate of 1.3 μL/s, followed by recirculating 20 μL back and forth for 40 times to emulate stirring conditions for 30 min. Finally, the biochip is washed by flowing 600 μL of running buffer at a flow rate of 1.3 μL/s.

FN grafting process (FNg): Before their use, the 1DPC biochips were immersed in 2% (3-aminopropyl) triethoxysilane in ethanol for 1 h at room temperature followed by sonication, washing in ethanol, and soft baking on a hot plate at 110 °C for 1 h. The biochips were then immersed in 2% glutaraldehyde in bicarbonate buffer for 1 h at room temperature (adding $NaCNBH_3$), followed by sonication and washing in deionized water. The 1DPC biochips were finally topped with a microfluidic cell [20] and mounted on the optical read-out system. Upon application of the same procedure described above for the FN adsorption process, FN is grafted at the surface by the APTES/ glutaraldehyde functionalization [37].

PRC adsorption process (PRCa)**:** After either adsorption or grafting of FN, 180 μL of the PRC solution were injected with a flow rate of 1.3 μL/s, followed by recirculating 20 μL back and forth for 40 times, for 30 min. Finally, the biochip is washed by flowing 600 μL of running buffer at a flow rate of 1.3 μL/s. AA and GA samples were thus prepared following this methodology.

PRC grafting process (PRCg)**:** Hermanson proposes a reaction in which a phosphate-containing compound (which was PRC in this case) reacts with EDC and immediately after with imidazole to create a phosphorimidazole intermediate

which will further react with an amine-containing compound (FN in this case) to create a phosphoramidate linkage [30]. In this work, in order to apply this procedure, the PRC solution was modified by adding 0.1 M EDC (ThermoFisher) and agitating for 5 min. Then, imidazole (Sigma Aldrich) was added in excess and agitated for 30 min. The solution of activated PRC, containing the phosphorimidazole intermediate, was then injected in previously adsorbed or grafted FN biochips, following the same procedure described for the PRC adsorption process reported above. As result of this methodology, AG and GG samples were prepared.

Labelling for FLUO operation

The resolution of the LF mode permitted the direct monitoring of the growth of the binary coating, since the signal depends only on the mass loading at the surface. However, as it is shown below, PRC could be hardly detected in such a manner. Indeed, both its size and its interaction with FN had prevented the successful characterization of PRC in previous works. Therefore, in the present research, the FLUO mode was used in order to evaluate the PRC content in all coating combinations, which requested to specifically label PRC by means of a dye fluorophore. To this aim, the following procedure after the deposition of the binary coatings was adopted. First, the biochips were allowed to react with Human C-reactive protein (CRP, antigen grade from Biodesign International) dissolved at 2.5 μg/mL in the running buffer, which was modified by adding $CaCl_2$ at 100 mM. As already reported by R. T. Lee et al. in 2002 [39], the PRC binding site shows a high affinity to the corona-like ligands of the CRP in presence of calcium ions. Therefore, if PRC is present, CRP forms a ternary coating. Second, a solution of a Dyomics 647 conjugated monoclonal antibody specific for CRP (a-CRP, EXBIO Antibodies) in the running buffer at 5 μg/mL was injected in the biochips, followed by washing with 500 μL of running buffer. This step permitted to label CRP (and hence PRC) with a dye that perfectly matches the spectral characteristics of our read-out system.

Two sets of four biochips were prepared. Every set contained the four combinations for the binary coating: AA, AG, GA, GG. The first set was labeled with CRP/a-CRP and assayed in the FLUO mode. The second set was labeled with running buffer/a-CRP and assayed to give a set of blank measurements.

FN/PRC coated surface characterization

Water contact angle: The wettability of the FN/PRC coated surfaces was assessed by static WCA measurements performed with a Video Contact Angle System VCA-2500 XETM (AST products Inc., Billerica, USA). 1 μL of deionized water was used. At least 3 areas per sample were measured and at least 2 different samples per condition were analyzed.

X-ray Photoelectron Spectroscopy: The chemical composition of the different FN/PRC coated surfaces was assessed by XPS (depth analysis of 5 nm). The analyses were carried out using an X-Ray Photoelectron Spectrometer (XPS-PHI 5600-ci Spectrometer Physical Electronics, Eden Prairie, USA). Survey spectra (0–1400 eV) were obtained using a standard aluminum X-ray source (1486.6 eV) at 300 W. The detection was performed at 45° with respect to the surface normal and the analyzed area was 0.005 cm^2. For the high-resolution spectra of the C1s peak, a standard magnesium X-ray source (Mg Kα = 1253.6 eV) was used at 150 W without charge neutralization but with energy referencing. The curve fitting procedure of the components underlying the C1s peaks was performed by means of a least-square minimization procedure employing Gaussian–Lorentzian functions and a Shirley-type background.

RESULTS

LF results on 1DPC biochips: The LF signal was recorded during the FN/PRC binary coating deposition steps previously described. At the beginning of the experiments, the fluidic channel was filled with the running buffer and the BSW resonance was tracked until a stable baseline was obtained. Fig. 2 shows the time traces of the sensorgram for the four coating combinations recorded during the FN/PRC binary coatings' growth. The traces are the average of the signals measured in 26 spots, each 230 μm wide (100 CCD rows), distributed along the illumination line. In the inset of Fig. 2, the experimental BSW resonance measured by the CCD in one spot is shown.

In the case of the AA combination, after stabilization at t = 3 min, FN solution was injected and an increase of the θ was observed until reaching a plateau at t ~ 15 min and Δθ ~ 110 pix. At t = 33 min, the adsorption of FN was stopped and running buffer was injected in order to wash. No change of Δθ was observed after washing process, indicating that no desorption of FN took place. At t = 43 min, PRC solution was injected. After an initial injection phase (first 2 min), the solution was recirculated back and forth across the sensitive area of the 1DPC biochip to improve molecular reactions with the surface and mimic stirring conditions. A first steep increase of Δθ, up to about 300 pix, was observed, which was mainly due to changes in refractive index after the addition of the PRC solution. During the PRC interaction (30 min), the LF signal slightly decreased. The small oscillations of the LF signal were introduced by pressure changes due to the recirculation procedure. When running buffer was injected to wash at t = 73 min, a decrease of Δθ down to a value of 42 pix was detected.

For the AG combination, a behavior similar to the AA case was observed after the injection of the FN solution. When the activated PRC solution was injected, the steep change of the LF signal due to the refractive index of the solution was much more pronounced than in the AA case, exceeding a value of 850 pix. This was due to the EDC and imidazole in the activated PRC solution, which increased the refractive index. Again, the LF signal slightly decreased during the PRC interaction (30 min). At t = 73 min, when running buffer was injected, Δθ dropped down to 79 pix.

In the case of the GA combination, after the injection of the FN solution, a faster increase of Δθ was observed with respect to the AA and AG cases. A plateau was observed at t = 10 min. No recovery was observed when the surface was washed with running buffer. After the injection of the PRC

solution, a similar behavior to the AA case was observed: a fast increase on the Δθ value until almost 300 pix. This value remained stable for 30 min, until the washing process, where it dropped down to 101 pix.

Finally, the GG combination showed a mixed behavior of the AG and GA cases. For the first step, where FN was injected, a very similar behavior to the GA case was observed (residual signal level of 105 pix). After adding the activated PRC solution, a large and steep increase of Δθ (about 800 pix) due to the change of the solution is observed during the PRC reaction. Then, the LF signal drops down to 112 pix after the washing process.

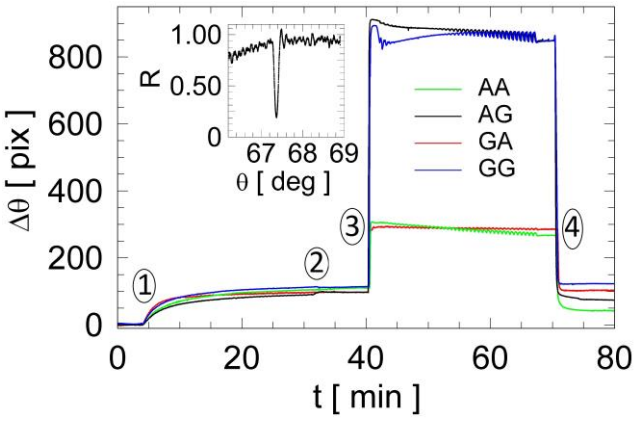

Figure 2: Temporal dependency of the BSW resonance relative angular position Δθ in CCD camera pixels recorded during the FN and PRC injection and recirculation. The curves were recorded for the four combinations of adsorption/grafting conditions. (1) FN injection; (3) PRC injection; (2) and (4) rinsing with running buffer. Inset: BSW resonance dip obtained by averaging 100 CCD rows.

Fig. 3 shows the values of the residual Δθ measured in running buffer after FN and PRC deposition, for the four binary coating combinations (left ordinate axis). Data were the average of the results obtained in two replicated experiments, carried out with two different 1DPC biochips. Data were converted to mass surface coverage (right *y*-axis) using De Feiter's equation [40] and $\partial n/\partial c = 0.187\ cm^3/g$ as refractive index increment of the biomolecules [41]. As it is observed in Fig. 3, AA and AG combinations yielded the highest FN coverage of the surface with values of (185 ± 2) ng/cm² and (184 ± 5) ng/cm², respectively. GA and GG showed a FN coverage of (160 ± 5) ng/cm² and (177 ± 6) ng/cm², respectively.

Fig. 3 also shows a striking difference when PRC was injected either on FNa or FNg conditions. For the AA and AG cases, clearly PRC caused desorption of FNa, decreasing the overall LF residual signal. In this case, it was not possible to quantify the PRC contribution to the LF signal and the PRC coverage. For the GA and GG cases, no FN loss was detected and PRC contributed to increase the residual LF signal. From the increase of the LF residual signal, it was possible to estimate a PRC coverage of (10 ± 5) ng/cm² and (12 ± 6) ng/cm² adsorbed and grafted, respectively, demonstrating that 1DPC biochips could successfully give an estimation of the presence of such a small biomolecule in LF mode. However, it should be considered the high uncertainty reported (1σ standard deviation), which resulted in measurements very close to the LoD, for such PRC coverage.

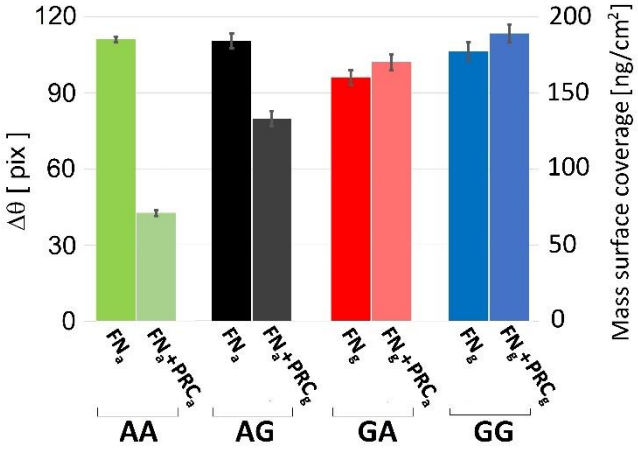

Figure 3: Residual angular shifts Δθ (left ordinate) after FN and after FN+PRC recorded after rinsing in running buffer. The values are the average values of those obtained with different chips in replicated experiments. Data were converted to mass surface coverage values (right *y*-axis).

FLUO results on 1DPC biochips: After the end of the LF part of an experiment, the PRC molecules bound at the 1DPC biochip surface by means of the protocol described above and making use of CRP/ a-CRP. In Fig. 4, for each combination, we show the angular fluorescence spectra recorded after labelling and in running buffer. For the same biochip, the spectra in 5 different spots distributed along the illumination line were recorded. Each spot corresponds to 100 CCD rows. Fluorescence spectra were acquired before (background) and after (signal) interaction with the labelled a-CRP. Then, the spectra were subtracted spot by spot to obtain background corrected signals. Curves in bold are the average of the spectra measured in the 5 spots. In all experiments we verified experimentally that the ratio of the TE and TM peak intensities is constant, indicating that there is no change of the orientational distribution of the emitters, which is assumed to be isotropic.

The blue curves correspond to experiments in which the biochips were effectively in contact with CRP during the labelling step. The grey curves were obtained from experiments in which the modified running buffer was injected instead of CRP for the grey spectra as negative control. Such latter spectra were used as a fluorescence blank to properly keep into account non-specific binding of CRP and a-CRP during the labelling step.

It is clear from Fig. 4 that the best conditions to include PRC in the binary coating were obtained when FN was grafted at the surface (Fig. 4c and 4d). For FNa, the absence of a FLUO signal (Fig. 4a and 4b) confirmed the LF result, i.e. that PRC did not bind at the surface but caused the desorption of FN. The increase of the blank spectral intensity from the GA to the GG case, indicated a specific role of the surface chemistry in the non-specific binding events.

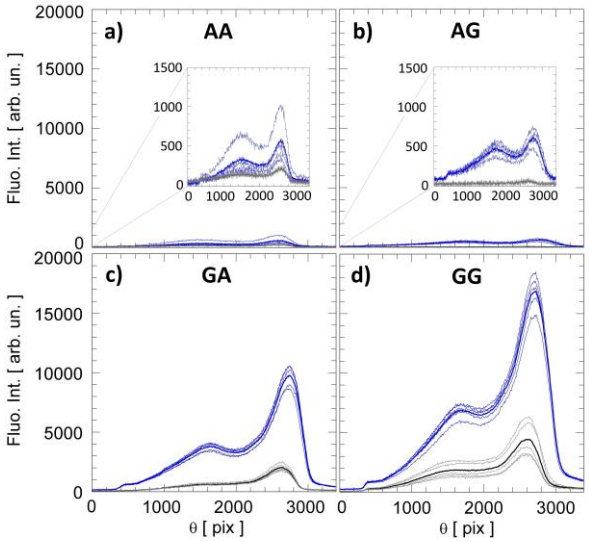

Figure 4: Angular FLUO intensities for the (a) AA, (b) AG, (c) GA and (d) GG cases. The insets in (a) and (b) show the signals in a smaller intensity range. (Blue curves) Signals recorded in 5 different spots for specifically labelled biochips. Average curve in bold blue). (Grey curves) Signals recorded in 5 different spots for non-specifically labelled biochips (blanks). The curves in bold are the average of the 5 spots.

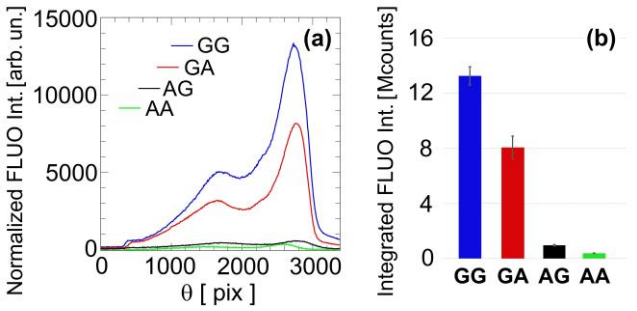

Figure 5: (a) Normalized angular fluorescence spectra and (b) their integrals, giving the integrated intensities, for the four coating combinations.

The average curves in bold shown in Fig. 4 were subtracted, signal to blank, to generate the normalized average fluorescence spectra shown in Fig. 5a, for the four binary coating combinations. As clearly shown in Fig. 5b, the integrated fluorescence intensities recorded in the GA (GA_{FLUO}) and GG (GG_{FLUO}) cases were well distinguished from the AA and AG cases. Such results permitted to unambiguously assess that PRC binds at the surface in the GA and GG cases, confirming the LF result, even if it was very close to the LoD in the latter. A larger integrated intensity in the GG case was observed, indicating that the PRC coverage is 38% larger with respect of the GA case. Moreover, the results showed that a residual amount of PRC in the AA and AG (more pronounced) cases could be detected, although these data are found within the error band.

WCA and XPS analysis: In order to further characterize the samples and to compare the results with previous investigations, WCA measurements as well as XPS survey and C1s high resolution analyses were performed. Such measurements were carried out making use of FN/PRC binary coatings deposited onto 1DPC chips by means of the same procedures used in the LF experiments.

Table 1: XPS survey analysis and water contact angle

Sample	Atomic composition				WCA
	C	O	N	Si	
SiO_2	29 ± 7	49 ± 5	ND	21 ± 4	ND
FNa	44 ± 8	36 ± 6	6.8 ± 0.8	14 ± 2	79 ± 6
AA	20 ± 4	54 ± 3	2.1 ± 0.4	24 ± 2	76 ± 8
AG	28 ± 3	48 ± 3	5 ± 2	18 ± 2	73 ± 7
FNg	64 ± 2	20.4 ± 0.9	12 ± 2	3.5 ± 0.3	90 ± 4
GA	62 ± 2	20.8 ± 0.5	12 ± 2	5 ± 1	62 ± 11
GG	59 ± 2	22 ± 2	12 ± 1	5 ± 2	62 ± 10

Table 1 shows the chemical composition and WCA of the surfaces, while Fig. 6 shows the high resolution spectra of C1s together with the respective WCA images. In the FNa condition, the increase in C and N amounts as well as the decrease in O and Si when compared to the SiO_2 surface evidenced the presence of the protein. The detection of the C-C and C-H bands in the high-resolution spectrum evidenced also the presence of the protein, since these chemical bonds are not present in the substrate. After the adsorption of PRC, namely AA, a decrease in the concentration of C and N as well as a decrease in the intensity of the bands corresponding to the protein in the high resolution spectrum indicated desorption of fibronectin. The same effect was observed for AG condition. No significant difference was observed on the WCA. In the case of FNg condition, higher amount of C and N were observed when compared to FNa condition, as well as higher intensity in the bands corresponding to the protein in the high resolution spectrum. These observations implied a more homogeneous coverage of the substrate in the case of FNg conditions. A higher WCA was observed when compared to FNa condition (90° and 79°, respectively). No significant changes in the chemical composition were observed after the addition of PRC -adsorbed or grafted - to FNg condition.

DISCUSSION

The FN/PRC coatings have been studied by the team of Mantovani et al. since 2011. However, in previous works only qualitative and semi-quantitative analysis could be performed. The results reported in the present work can be compared to the literature. Indeed, the quick adsorption of FN observed in the first 10 min of contact of the solution with the surface is coherent with several observations of different research groups on model surfaces [42]. Indeed, Pauthe et al. have already demonstrated that more than 80% of FN is adsorbed during the first 5 min of contact with a hydrophilic surface. Moreover, the stability of the adsorption after washing with buffer solution was also previously reported [43]. The high increase in the mass deposited after the addition of PRC, followed by a great decrease after washing, was previously observed in preliminary tests with Quartz Crystal Microbalance and Surface Plasmon Resonance (data

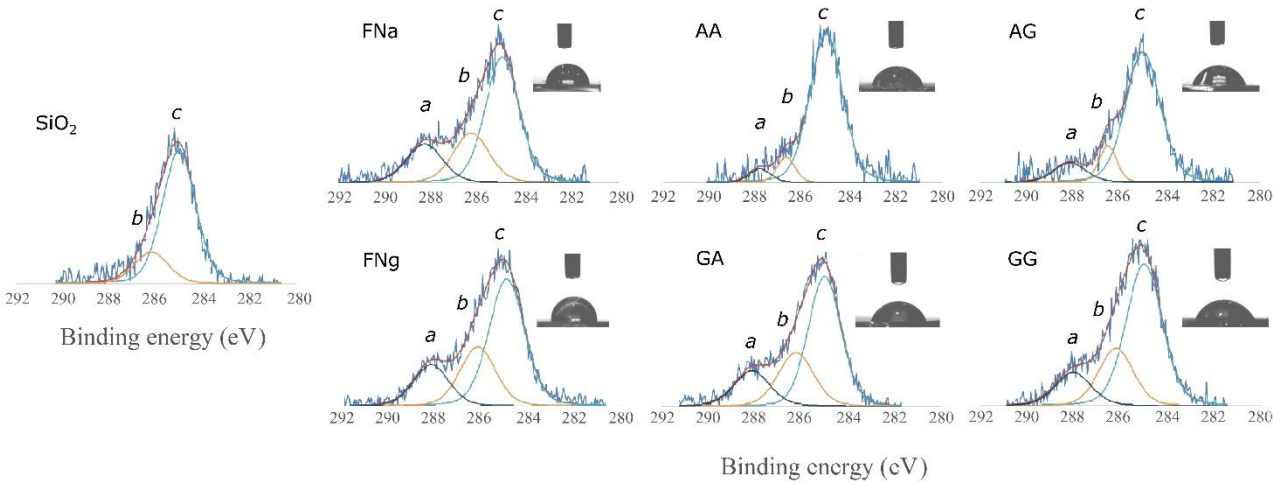

Figure 6: High resolution analysis of C1s for FNa, AA, AG, FNg, GA, GG and the substrate SiO_2. a) 288.2 eV: O-C=O/N-C=O; b) 286.5 eV: C-OH/C-N/C-O; c) 285 eV: C-C/C-H. Each spectrum is complemented by the respective WCA image.

Surface Plasmon Resonance (data not shown). The desorption of the protein after the addition of PRC as well as its high stability when grafted was also previously discussed on fluorocarbon surfaces [7,12]. This fact implies that, no matter the nature of the substrate, the grafting process of FN leads to a stable coating. Concerning the mass coverage of FN, the values obtained are coherent with previous quantifications of FN coatings in hydrophilic surfaces, as the SiO_2 used here [42]. In addition, a covering of around 160 ng/cm^2 implies a monolayer of FN in an elongated conformation of the protein, which is also in accordance with previous reported data [42,44]. Moreover, the difference observed in the WCA has already indicated both higher homogeneity of the FNg coating and different conformation of the protein when compared to FNa, as previously reported [43]. Regarding the interaction of PRC with FN coatings, previous data speculated about desorption of the protein in the FNa condition after the addition of PRC. In this work, it was possible to estimate a loss in mass of the protein of 114 ng/cm^2 in the case of AA and 51 ng/cm^2 for AG. Hence, through the technique used here, it was possible to complement and confirm previous works in a quantitative way. It should be noticed that the main drawback of the LF approach is that it failed to quantify PRC when a desorption of the proteins was observed (higher amount of PRC in the final surface without recording any particular signal in LF sensorgrams), mainly because the mass detection is not specific for a molecule. Furthermore, in the present works, the evaluation of the PRC surface coverage can be also affected by a different biomolecule refractive index increment ($\partial n/\partial c$) that could be slightly different between large (FN) and small (PRC) molecules. Such effects can be lowered when considering the fluorescence signals and the ability, through a specific fluorescent species, to reach PRC-CRP complexes inside the FN matrix. The larger difference in the GA_{FLUO} and GG_{FLUO} seemed to attest a better discrimination between the GA and GG cases, mainly due to the use of labelled a-CRP. Hence, it was possible not only to assess the presence of PRC but also to estimate the mass coverage, which was not possible with previous characterizations.

Concerning the biological performances of the coatings, the stimulation of the endothelialization process (FN) and hemocompatibility (PRC) have been reported elsewhere; however, the discussion about these results can be complemented by the observations made in the present work. Indeed, previous works have shown no difference in endothelial cell viability on AA, AG and GA conditions, with significant lower viability on GG samples [7]. In contrast, GA condition presented the highest hemocompatibility. Regarding the results in cell viability, they can be explained by: 1) a conformation of FN that permits the RGD sequence to interact with cells in AA, AG and GA conditions; 2) the highest amount of PRC found in GG condition - most probably in deeper layers - which avoids the RGD sites to be available (possible formation of macromolecular complexes as previously reported). Finally, in the case of hemocompatibility, the findings can be justified by: 1) the higher stability of FN grafted when in contact with PRC, 2) a higher amount of PRC in FNg coatings and 3) a better organization of PRC at the surface in GA condition when compared to GG. Further investigations are required to better understand the nature of the interaction of the molecules. Moreover, the changes in conformation of the protein/formation of macromolecular complexes should be studied; mainly because they would have an impact on the availability of the cell binding domain and in the organization of PRC at the surface.

CONCLUSIONS

In this work, it has been shown that 1DPC biochips sustaining BSW are a powerful tool for surface characterization of interactions of biomolecules with different molecular weight. In particular, by exploiting a combined LF and FLUO approach, the quantification of FN and PRC molecules for different coatings combining adsorption and grafting processes has been achieved. Moreover, a higher stability of FN grafted - compared to the adsorbed one - when in contact

with PRC has been confirmed. The quantitative characterization was coherent with previous qualitative and biological evaluations, making this technique a promising one for the characterization of binary coatings containing low molecular weight molecules with relevant properties for biomaterial applications.

ACKNOWLEDGMENT

The authors would like to express their gratitude for their collaboration on the characterization and/or their technical assistance to Pascale Chevallier, PhD and Stéphane Turgeon, PhD. The authors would like to thank Sara Proietti, PhD and Elisabetta Sepe from SAPIENZA for their technical assistance during the experiments and Ambra Giannetti, PhD and Francesco Baldini, PhD from IFAC-CNR for providing biochemical reagents used in the fluorescence characterizations. F.C. wishes to acknowledge the European Community in the framework of ERANET Cofound action PhotonicSensing 2016 for the project "OPTIMO" (Optical fiber device for simultaneous manometry, pH-metry and bilimetry in oesophagus, DIT.AD010.027).

Author Contributions

The manuscript was written through contributions of all authors. All authors have given approval to the final version of the manuscript. Authors AS and VMM contributed equally.

REFERENCES

(1) Jones, J. R. Observing Cell Response to Biomaterials. *Mater. Today* **2006**, *9* (12), 34–43.

(2) Tang, L.; Thevenot, P.; Hu, W. Surface Chemistry Influences Implant Biocompatibility. *Curr. Top. Med. Chem.* **2008**, *8* (4), 270–280.

(3) Lin, Q.; Yan, J.; Qiu, F.; Song, X.; Fu, G.; Ji, J. Heparin/Collagen Multilayer as a Thromboresistant and Endothelial Favorable Coating for Intravascular Stent. *J. Biomed. Mater. Res. - Part A* **2011**, *96 A* (1), 132–141.

(4) Li, G.; Yang, P.; Qin, W.; Maitz, M. F.; Zhou, S.; Huang, N. The Effect of Coimmobilizing Heparin and Fibronectin on Titanium on Hemocompatibility and Endothelialization. *Biomaterials* **2011**, *32* (21), 4691–4703.

(5) Tardif, K.; Cloutier, I.; Miao, Z.; Lemieux, C.; St-Denis, C.; Winnik, F. M.; Tanguay, J.-F. A Phosphorylcholine-Modified Chitosan Polymer as an Endothelial Progenitor Cell Supporting Matrix. *Biomaterials* **2011**, *32* (22), 5046–5055.

(6) Chen, J.; Chen, C.; Chen, Z.; Chen, J.; Li, Q.; Huang, N. Collagen/Heparin Coating on Titanium Surface Improves the Biocompatibility of Titanium Applied as a Blood-Contacting Biomaterial. *J. Biomed. Mater. Res. - Part A* **2010**, *95 A* (2), 341–349.

(7) Montaño-Machado, V.; Noël, C.; Chevallier, P.; Turgeon, S.; Houssiau, L.; Pauthe, E.; Pireaux, J.-J.; Mantovani, D. Interaction of Phosphorylcholine with Fibronectin Coatings: Surface Characterization and Biological Performances. *Appl. Surf. Sci.* **2016**, *396*, 1613–1622.

(8) Hindié, M.; Camand, E.; Agniel, R.; Carreiras, F.; Pauthe, E.; Van Tassel, P. Effects of Human Fibronectin and Human Serum Albumin Sequential Adsorption on Preosteoblastic Cell Adhesion. *Biointerphases* **2014**, *9* (2), 029008 1-9.

(9) He, T.; Yang, Z.; Chen, R.; Wang, J.; Leng, Y.; Sun, H.; Huang, N. Enhanced Endothelialization Guided by Fibronectin Functionalized Plasma Polymerized Acrylic Acid Film. *Mater. Sci. Eng. C* **2012**, *32* (5), 1025–1031.

(10) Lewis, A. L.; Hughes, P. D.; Kirkwood, L. C.; Leppard, S. W.; Redman, R. P.; Tolhurst, L. a.; Stratford, P. W. Synthesis and Characterisation of Phosphorylcholine-Based Polymers Useful for Coating Blood Filtration Devices. *Biomaterials* **2000**, *21* (18), 1847–1859.

(11) Nakabayashi, N.; Williams, D. F. Preparation of Non-Thrombogenic Materials Using 2-Methacryloyloxyethyl Phosphorylcholine. *Biomaterials* **2003**, *24* (13), 2431–2435.

(12) Montaño-Machado, V.; Chevallier, P.; Mantovani, D.; Pauthe, E. On the Potential for Fibronectin/Phosphorylcholine Coatings on PTFE Substrates to Jointly Modulate Endothelial Cell Adhesion and Hemocompatibility Properties. *Biomatter* **2015**, *5* (1).

(13) Turner, C. J.; Badu-Nkansah, K.; Hynes, R. O. Endothelium-Derived Fibronectin Regulates Neonatal Vascular Morphogenesis in an Autocrine Fashion. *Angiogenesis* **2017**, *20* (4), 519–531.

(14) Yang, D.; Lü, X.; Hong, Y.; Xi, T.; Zhang, D. The Molecular Mechanism of Mediation of Adsorbed Serum Proteins to Endothelial Cells Adhesion and Growth on Biomaterials. *Biomaterials* **2013**, *34* (23), 5747–5758.

(15) Goda, T.; Konno, T.; Takai, M.; Moro, T.; Ishihara, K. Biomimetic Phosphorylcholine Polymer Grafting from Polydimethylsiloxane Surface Using Photo-Induced Polymerization. *Biomaterials* **2006**, *27* (30), 5151–5160.

(16) Chevallier, P.; Janvier, R.; Mantovani, D.; Laroche, G. In Vitro Biological Performances of Phosphorylcholine-Grafted EPTFE Prostheses through RFGD Plasma Techniques. *Macromol. Biosci.* **2005**, *5* (9), 829–839.

(17) Sinibaldi, A.; Sampaoli, C.; Danz, N.; Munzert, P.; Sibilio, L.; Sonntag, F.; Occhicone, A.; Falvo, E.; Tremante, E.; Giacomini, P.; et al. Detection of Soluble ERBB2 in Breast Cancer Cell Lysates Using a Combined Label-Free/Fluorescence Platform Based on Bloch Surface Waves. *Biosens. Bioelectron.* **2017**, *92* (February), 125–130.

(18) Yeh, P.; Yariv, A.; Hong, C.-S. Electromagnetic Propagation in Periodic Stratified Media I General Theory*. *J. Opt. Soc. Am.* **1977**, *67* (4), 423–438.

(19) Farmer, A.; Friedli, A. C.; Wright, S. M.; Robertson,

W. M. Sensors and Actuators B : Chemical Biosensing Using Surface Electromagnetic Waves in Photonic Band Gap Multilayers. *Sensors Actuators B. Chem.* **2012**, *173*, 79–84.

(20) Rizzo, R.; Alvaro, M.; Danz, N.; Napione, L.; Descrovi, E.; Schmieder, S.; Sinibaldi, A.; Chandrawati, R.; Rana, S.; Munzert, P.; et al. Bloch Surface Wave Label-Free and Fluorescence Platform for the Detection of VEGF Biomarker in Biological Matrices. *Sensors Actuators, B Chem.* **2018**, *255*, 2143–2150.

(21) Santi, S.; Barakat, E.; Descrovi, E.; Neier, R.; Peter, H.; Bellevaux, A. De. Real-Time Protein Aggregation Monitoring with a Bloch Surface Wave- Based Approach. **2014**, *9129*, 1–9.

(22) Hartstein, A.; Kirtley, J. R.; Tsang, J. C. Enhancement of the Infrared Absorption from Molecular Monolayers with Thin Metal Overlayers. **1980**, *45* (3), 201–204.

(23) Homola, J. Surface Plasmon Resonance Sensors for Detection of Chemical and Biological Species. *Chem. Rev.* **2008**, *108* (2), 462–493.

(24) Sinibaldi, A.; Danz, N.; Descrovi, E.; Munzert, P.; Schulz, U.; Sonntag, F.; Dominici, L.; Michelotti, F. Direct Comparison of the Performance of Bloch Surface Wave and Surface Plasmon Polariton Sensors. *Sensors Actuators, B Chem.* **2012**, *174*.

(25) Konopsky, V. N.; Alieva, E. V. Photonic Crystal Surface Waves for Optical Biosensors. *Anal. Chem.* **2007**, *79* (12), 4729–4735.

(26) Sinibaldi, A.; Anopchenko, A.; Rizzo, R.; Danz, N.; Munzert, P.; Rivolo, P.; Frascella, F.; Ricciardi, S.; Michelotti, F. Angularly Resolved Ellipsometric Optical Biosensing by Means of Bloch Surface Waves. *Anal. Bioanal. Chem.* **2015**, *407* (14), 3965–3974.

(27) Ye, J. Y.; Ishikawa, M. Enhancing Fluorescence Detection with a Photonic Crystal Structure in a Total-Internal-Reflection Configuration. *Opt. Lett.* **2008**, *33* (15), 1729–1731.

(28) Shen, H.; Wang, Z.; Wu, Y.; Yang, B. One Dimensional Photonic Crystals: Fabrication, Responsiveness and Emerging Applications in 3D Construction. *RSC Adv.* **2015**, *6*, 4505–4520.

(29) Joannopoulos, J. D.; Johnson, S. G.; Winn, J. N.; Meade, R. D. *Photonic Crystals: Molding the Flow of Light*, Second edi.; Princeton University Press: Princeton, New Jersey, USA, 2008.

(30) Raether, H. *Surface Plasmons*; Springer-Verlag: Berlin, 1988.

(31) Sinibaldi, A.; Fieramosca, A.; Rizzo, R.; Anopchenko, A.; Danz, N.; Munzert, P.; Magistris, C.; Barolo, C.; Michelotti, F. Combining Label-Free and Fluorescence Operation of Bloch Surface Wave Optical Sensors. *Opt. Lett.* **2014**, *39* (10).

(32) Michelotti, F.; Rizzo, R.; Sinibaldi, A.; Munzert, P.; Wächter, C.; Danz, N. Design Rules for Combined Label-Free and Fluorescence Bloch Surface Wave Biosensors. *Opt. Lett.* **2017**, *42* (14).

(33) Danz, N.; Sinibaldi, A.; Michelotti, F.; Descrovi, E.; Munzert, P.; Schulz, U.; Sonntag, F. Improving the Sensitivity of Optical Biosensors by Means of Bloch Surface Waves. *Biomed. Tech.* **2012**, *57* (SUPPL. 1 TRACK-E), 584–587.

(34) Sinibaldi, A.; Fieramosca, A.; Rizzo, R.; Anopchenko, A.; Danz, N.; Munzert, P.; Magistris, C.; Barolo, C.; Michelotti, F. Combining Label-Free and Fluorescence Operation of Bloch Surface Wave Optical Sensors. *Opt. Lett.* **2014**, *39* (10), 2947–2950.

(35) Danz, N.; Sinibaldi, A.; Munzert, P.; Anopchenko, A.; Förster, E.; Schmieder, S.; Chandrawati, R.; Rizzo, R.; Heller, R.; Sonntag, F.; et al. Biosensing Platform Combining Label-Free and Labelled Analysis Using Bloch Surface Waves. *SPIE Opt. + Optoelectron.* **2015**, *9506*, 95060V.

(36) Poulouin, L.; Gallet, O.; Rouahi, M.; Imhoff, J. M. Plasma Fibronectin: Three Steps to Purification and Stability. *Protein Expr. Purif.* **1999**, *17* (1), 146–152.

(37) Chang, Y.; Lee, W.; Feng, S.; Huang, H.; Lin, C. In Vitro Analysis of Fibronectin-Modified Titanium Surfaces. **2016**, 1–12.

(38) Hermanson, G. *Bioconjugate Techniques*, First edit.; Academic, Press:, Eds.; Elsevier: San Diego, CA;, 1996.

(39) Lee, R. T.; Takagahara, I.; Lee, Y. C. Mapping the Binding Areas of Human C-Reactive Protein for Phosphorylcholine and Polycationic Compounds. Relationship between the Two Types of Binding Sites. *J. Biol. Chem.* **2002**, *277* (1), 225–232.

(40) De Feijter, J. A.; Benjamins, J.; Veer, F. A. Ellipsometry as a Tool to Study the Adsorption Behavior of Synthetic and Biopolymers at the Air–water Interface. *Biopolymers* **1978**, *17* (7), 1759–1772.

(41) Vörös, J. The Density and Refractive Index of Adsorbing Protein Layers. *Biophys. J.* **2004**, *87* (1), 553–561.

(42) Baujard-Lamotte, L.; Noinville, S.; Goubard, F.; Marque, P.; Pauthe, E. Kinetics of Conformational Changes of Fibronectin Adsorbed onto Model Surfaces. *Colloids Surfaces B Biointerfaces* **2008**, *63* (1), 129–137.

(43) Montaño-Machado, V.; Hugoni, L.; Díaz-rodríguez, S.; Tolouei, R.; Pauthe, E.; Mantovani, D. A Comparison of Adsorbed and Grafted Fibronectin Coatings under Static and Dynamic Conditions. *PCCP* **2016**, *18*, 24704–24712.

(44) Bergkvist, M.; Carlsson, J.; Oscarsson, S. Surface-Dependent Conformations of Human Plasma Fibronectin Adsorbed to Silica, Mica, and Hydrophobic Surfaces, Studied with Use of Atomic Force Microscopy. *J Biomed Mater Res A* **2003**, *64* (2), 349–356.

Abstract graphic